Highly Sensitive Directional Torsion Sensor Based on a Helical Panda Fiber Taper

Yong-Qin Zhu, Yong-Sen Yu, Yang Zhao, Qi Guo, Xin-Yu Ming, Cheng-Xiu Lei, and Hong-Bo Sun, *Fellow, IEEE*

***Abstract*— A novel directional torsion sensor based on a helical taper is proposed and experimentally demonstrated. The helical taper was fabricated in panda polarization-maintaining fiber by electric-arc discharge of a fusion splicer and by rotating one end fiber clamp simultaneously. The optimal parameters of the taper are the waist diameter of 60.84 μm and the length of 700 μm. This torsion sensor has a sensitivity of −3.191 nm/(rad/m) in the twist rate ranges from 0 to 13.57 rad/m, which is relatively higher than the value so far reported. Then, the torsion sensor also has the ability to identify rotational direction. In addition, the helical taper is almost insensitive to temperature.**

***Index Terms*— Fiber optic sensors, helical taper, torsion sensors, polarization-maintaining fiber.**

I. Introduction

THE optical fiber sensors have the advantages of small size, light mass and anti-electromagnetic interference, which have attracted great interest in many fields [1], [2]. For example, a holographic control method for light propagations in complex media was proposed recently, which enables multimode fiber to be used as an ultra-narrow imaging tool [3]. And the multimode optical fiber transmission based on deep learning networks have also been studied [4]. Torsion is an important mechanical parameter, and various torsion sensors can be embedded in engineering structures for shape detection and structural health monitoring [5]. In the past few decades, various fiber torsion sensors have been investigated, for example, helical Long Period Gratings (hLPGs) [6]–[8], and variety of optical fiber interferometers [9]–[11]. The hLPGs-based torsion sensors have great mechanical strength, as early as 2004, Wang et al proposed using long period grating to measure twist angle and distinguish the rotational direction [12]. Recently, Cao et al fabricated a helical Long Period Gratings (hLPGs) in double-clad fiber by CO_2 laser [13]. The hLPGs structure has relatively high twist sensitivity that up to ∼0.384 nm/(rad/m), which is the highest sensitivity in the reported hLPGs at present. In 2015, a pre-twist taper in polarization-maintaining fiber was proposed [14]. In this SMF-PMF-SMF sandwich structure, besides the axial force, a pre-twist stress was also applied before discharging, which generate spiral in the tapered transition zones after pulling. In addition, the response of the interference peaks to torsion is different, and an appropriate peak must be chosen for torsion sensing. Another Tan et al firstly reported a taper structure based on multicore fiber, which has a tunable torsion sensitivity between 0.12 nm/°∼1.00 nm/° [15] and the angle measurement ranges from 160° to 940°. However, to the best of our knowledge, most of the torsion sensors so far reported are unable to ensure high sensitivity and identify rotational direction simultaneously. Furthermore, many torsion sensors are sensitive to temperature [16], [17], which have the problem of torsion-temperature cross sensitivity.

In this letter, we propose a novel helical taper structure, which is fabricated in panda polarization-maintaining fiber by an electric-arc discharge method. Due to the rotation of fiber clamp when tapering, the two stress regions of panda fiber show as a helical shape in the waist, which enhances the coupling between different modes and improves the torsion sensitivity. Additionally, this helical taper sensor has a high torsion sensitivity, a low temperature sensitivity and an ability to identify rotational direction. Moreover, the fabrication process of the helical taper is simple, and the cost of an arc discharge method is also greatly low, which does not require expensive femtosecond laser equipment, etc.

II. Fabrication

The device diagram of fabricating this helical taper is illustrated in Fig. 1(a). Firstly, one panda fiber (PMF1550, 125-13/250) with coating removed was placed in the V-groove of a fusion splicer (Ericsson FSU-995PM) straightly, and fixed by fiber clamps. Then, one user-defined taper program was selected. There are three steps, PULL1, PULL2 and PULL3, and the discharge time and discharge current of each step are different. Additionally, when the helical taper was fabricated by arc discharge, the discharge time and current must be chosen appropriately. If the discharge current is too small, the taper can't be drawn, and if it is too large, the taper is easily blown. What's more, the discharge time must be also greatly controlled to obtain a better spectrum. Finally, by constantly changing the discharge time and current, and comparing the

Manuscript received March 13, 2019; revised April 15, 2019; accepted May 4, 2019. Date of publication May 9, 2019; date of current version June 12, 2019. This work was supported in part by the National Natural Science Foundation of China and in part the National Key Research and Development Program of China under Grant 2017YFB1104300, Grant 91860140, Grant 61825502, Grant 61590930, and Grant 61435005. *(Corresponding author: Yong-Sen Yu.)*

Y.-Q. Zhu, Y.-S. Yu, Y. Zhao, Q. Guo, X.-Y. Ming, and C.-X. Lei are with the State Key Laboratory of Integrated Optoelectronics, College of Electronic Science and Engineering, Jilin University, Changchun 130012, China (e-mail: yuys@jlu.edu.cn).

H.-B. Sun is with the State Key Laboratory of Integrated Optoelectronics, College of Electronic Science and Engineering, Jilin University, Changchun 130012, China, and also with the State Key Laboratory of Precision Measurement and Instruments, Department of Precision Instrument, Tsinghua University, Beijing 100084, China.

Color versions of one or more of the figures in this letter are available online at http://ieeexplore.ieee.org.

Digital Object Identifier 10.1109/LPT.2019.2915918

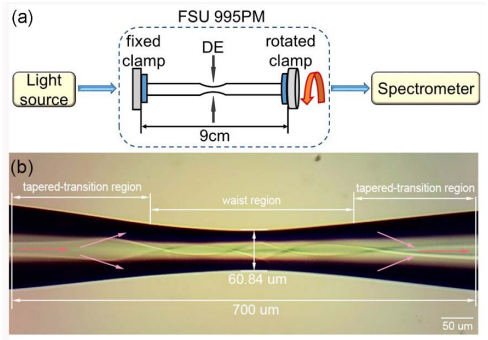

Fig. 1. (a) The experimental diagram of fabricating the helical taper. (b) The optical micrograph of this helical taper with waist diameter of 60.84μm and the length of 700μm.

output spectra under different parameters, the optimal parameters are obtained as follows: fusion time1 = 9s, fusion current1 = 15mA; fusion time2 = 7s, fusion current2 = 12mA; fusion time3 = 2s, fusion current3 = 7mA. Furthermore, in these three discharge steps, the first step is mainly to make the optical fiber thinner, and there is no rotation in the step. Then, when the taper program proceeded to the second step, a 360° twist stress was applied to the fiber by rotating the rigth side fiber clamp. Since the pulling and twist are simultaneously performed, the force is mainly concentrated in the thin taper waist, as demonstrated in Fig. 1(b). Finally, the third step is to shape the helical taper through a small current and short-time discharge, and there is also no rotation.

As shown in Fig. 1(a), the transmission spectrum is recorded by a spectrometer (Yokogawa AQ6370B), and a broadband light source (Superk Compact, NKT Photonics, Inc.) outputs supercontinuous light with a wavelength ranges from 600 nm to 1700 nm. The Fig. 1(b) is the optical micrograph of the helical taper. Then, using the dimension measurement software ImageJ and the proportional conversion, the waist diameter and the length of the helical taper can be got as 60.84 μm and 700 μm, respectively. As obviously shown in Fig. 1(b), because of a rotation of one side fiber clamp during pulling, the two stress regions are helical shape in the waist after discharging. And in this helical taper, there are mainly two sets of interferences [18], [19]. Firstly, the fundamental mode HE_{11} and the excited higher-order mode HE_{21} will be coupled to each other. And as shown in Fig. 1(b), when the light propagates to the first tapered-transition region, as the diameter of the fiber is tapered, a portion of core mode is coupled to the cladding, forming the cladding mode. Then, in the second tapered-transition region, the cladding mode is recoupled back to the core and interferes with the core mode, which form Mach-Zehnder interference. In addition, because of the twist stress applied on the cross section of panda fiber, the original two orthogonal polarization modes HE_{11}^{x} and HE_{11}^{y} will also be coupled, which form polarization interference.

The Fig. 2(a) demonstrated the transmission spectrum of this helical taper with an insertion loss of ~11 dB, and a maximum extinction ratio reaches to ~12 dB at 1630 nm. In the transmission spectrum, DipA is labeled mainly for the following torsion and temperature experiments. As shown

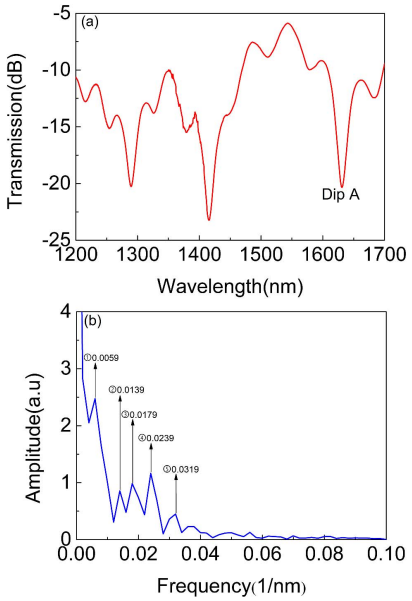

Fig. 2. (a) Transmission spectrum of the helical taper. (b) FFT spectrum of the transmission spectrum.

in Fig. 2(a), we can clearly observe that there are two sets of interference spectra. According to the mode coupling is determined by the mode profile and the amplitude of the axial mode field, and combined with the symmetry of the mode field, we can get that the weak interference peaks are generated by the coupling between HE_{11} and HE_{21}, and the strong peaks are generated by the coupling between the two orthogonal fundamental modes HE_{11}^{x} and HE_{11}^{y}. Subsequently, the transmission spectrum was subjected to fast Fourier transform (FFT), and the spatial frequency spectrum was obtained. In the spectrum that illustrated in Fig. 2(b), the strongest peak ① represents the interaction between two orthogonal fundamental modes, and the peak ④ indicates the interaction between the HE_{11} and HE_{21}. Additionally, according to the formula that $\varepsilon = \Delta n_{eff} l/\lambda^2$ [10], the effective refractive indices difference between HE_{11}^{x} and HE_{11}^{y} can be calculated as 0.0202, and the Δn_{eff} between HE_{11} and HE_{21} is 0.0820. Besides, the helical taper also causes additional mode crosstalk, coupling also occurs between different modes of each polarization state. As the peaks ② ③ and ⑤ shown in Fig. 2(b), there are a series of weaker frequency terms in the spatial frequency spectrum.

III. Theory

When a beam of light transmits along the helical taper, coupling occurs between the different modes, and forming interference fringes. Since the length of the helical taper is relatively short, the coupling between HE_{11} and HE_{21} is weak. Here, we mainly consider the coupling between two orthogonal fundamental modes, which is HE_{11}^{x} and HE_{11}^{y}. The output light intensity formed by two orthogonal fundamental modes is written as:

$$I = I_x + I_y + 2\sqrt{I_x I_y}\cos\left(\Delta\Phi_{xy}\right) \tag{1}$$

where I_x and I_y are the light intensity of HE_{11}^{x} and HE_{11}^{y} modes $\Delta\Phi_{xy}$ is the phase difference between the

corresponding modes. In addition, $\Delta\Phi_{xy}$ is demonstrated as:

$$\Delta\Phi_{xy} = 2\pi \left(n_{eff}^{x} - n_{eff}^{y}\right) \mathrm{L}/\lambda \tag{2}$$

where n_{eff}^{x} and n_{eff}^{y} are the effective refractive indices of the two orthogonal fundamental modes, L is the effective length of this helical taper, and λ is the input light wavelength. When $\Delta\Phi_{xy} = (2m+1)\pi$, there are a series of attenuation peaks, and the wavelength of peaks can be written as:

$$\lambda_m = 2\left(n_{eff}^{x} - n_{eff}^{y}\right) \mathrm{L}/(2\mathrm{m}+1) \tag{3}$$

where m is the interference order and it is an integer. To the best of our knowledge, when the cross section of a panda fiber is pressed in any direction, the fast and slow axis will be changed, and the original two orthogonal fundamental modes are coupled. The coupled intensity is determined by the magnitude and direction of the force, and the length of stressed fiber [20]. As shown in Fig. 1(a), when the panda fiber is tapered, a transverse shear force is applied by rotating one side fiber, therefore, HE_{11}^{x} and HE_{11}^{y} modes will be coupled to form interference fringes.

According to the photo-elastic effect, the effective refractive index (ERI) will change with the increasing of twist rate [21]. A permanent twist rate τ_0 was induced into the panda fiber when fabricated the helical taper, which leads to the modulation of ERI. And according to [21], the relationship between ERI and twist rate is as follows: $n(\tau) = n_0\rho^2\left[1 + (\tau \pm \tau_0)^2/2\right]$, where n_0 is the original refractive index, ρ is the radius of panda fiber, and τ is the twist rate applied when pulling. The "+" and "−" means applied twist in clockwise and counter clockwise direction, respectively. Additionally, when a twist stress is applied to a cylindrical structure composed of two concentric and different materials, the relationship between the stresses applied to each section is written as:

$$\frac{\sigma_{core}}{\sigma_{cladding}} = \frac{\mu_{core} d_{core}}{\mu_{cladding} d_{cladding}} \tag{4}$$

where σ_{core} and $\sigma_{cladding}$ are the torsion stress applied between core and cladding, μ_{core} and $\mu_{cladding}$ are the shear modulus corresponding to core and cladding, and the d_{core} and $d_{cladding}$ are the corresponding diameter. Since the diameter of cladding is much larger than the core, and the shear modulus of core and cladding are similar. So the effect of the applied twist stress for the core can be disregarded by Eq.(4). Therefore, the ERI of fiber core caused by the torsion is almost unchanged.

According to Eq.(3) and the relationship between effective refractive index n and the twist rate τ, we can derive the following relation between $\Delta\lambda$ and $\Delta\tau$:

$$\Delta\lambda = \frac{-2Ln_{eff}^{cl,f/s}\rho_{cl}^{2}(\tau \pm \tau_0)}{2m+1}\Delta\tau \tag{5}$$

where $n_{eff}^{cl,f/s}$ is the original effective refractive index of cladding along fast axis and slow axis, ρ_{cl} is the radius of cladding. As mentioned above, the symmetry of the helical taper is destroyed by the applied twist stress τ_0, which leads to this structure can identify the rotational direction. Therefore,

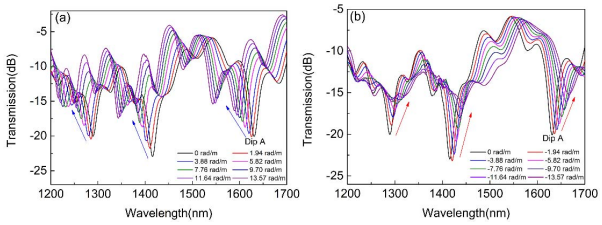

Fig. 3. (a) The transmission spectra shift with the increasing of twist rate in clockwise. (b) Transmission spectra shift with the increasing of twist rate in counter clockwise.

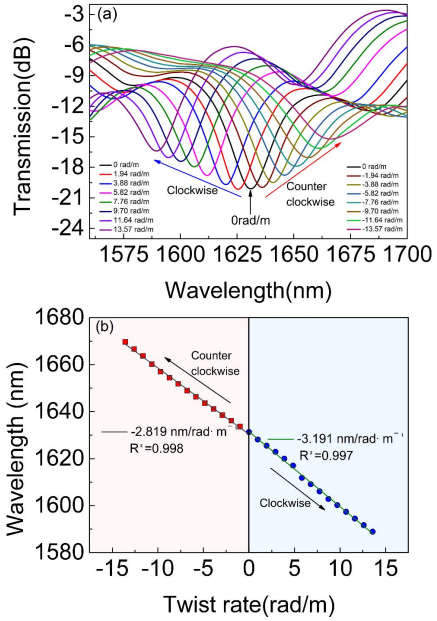

Fig. 4. (a) Transmission spectrum of Dip A shift with the increasing of twist rate in clockwise and counter clockwise. (b) Relationship of Dip A between the wavelength and twist rate.

the dips shift to short wavelength direction with the twist rate increasing in clockwise, and the wavelength occurs opposite shift when in counter clockwise. Here, the clockwise means the applied twist stress τ_0 direction when fabricated the helical taper, as the direction that shown in Fig. 1(a). And the opposite direction is defined as the counter clockwise.

IV. Experimental Results and Discussion

Firstly, the torsion characteristic of the helical taper was investigated. The helical taper was placed in the v-groove carefully, and ensure that it's not bent. Then one fiber clamp was fixed and the other can be rotated in clockwise and counter clockwise directions. And the angle step of rotation was set to 5° corresponding to a twist rate step of 0.970 rad/m. Here, the twist rate is defined as: $\tau = \alpha/L_0$, where τ is the twist rate, α is the twist radian of the fiber, and L_0 is the length between the two fiber clamps. The effective length L_0 is 9cm. Subsequently, the helical taper was rotated in clockwise and counter clockwise direction, respectively.

As shown in Fig. 3, with the changing of twist rate in clockwise and counter clockwise, all transmission peaks have a monotonous shift, which indicates that all peaks have the same response to torsion. And the Fig. 4 specifically demonstrates the changing of DipA when twist rate ranged

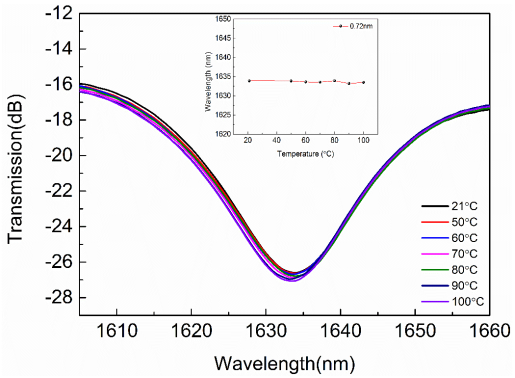

Fig. 5. The transmission spectrum of Dip A changes with different temperatures. Inset: wavelength of Dip A changes with temperature.

from −13.57 rad/m to 13.57 rad/m. It can be clearly observed that with the increasing of twist rate in clockwise, the transmission wavelength of DipA shifts linearly to short wavelength direction, which occurs "blue shifted"; when the twist rate increased in counter clockwise, transmission wavelength has opposite shift. Therefore, according to the wavelength has contrary shift when the helical taper in different torsional directions, we can identify the rotational direction. And by comparing with the theoretical analysis mentioned above, experimental results are in great agreement with the theoretical data. Then by linearly fitting the experimental data, as shown in Fig. 4(b), the torsion sensor reaches a high sensitivity up to −3.191 nm/(rad/m) with the R-square of 0.997, and this sensitivity is relatively higher than the values previous reported.

Then, the temperature response of the helical taper also was investigated. Firstly, the helical taper was fixed in the center of a heating table. And in order to ensure accuracy of the experiment, a cover was placed on the heating table to maintain a constant temperature. In the measurement, temperature was gradually increased from room temperature (21°C) to 100°C with a step of 10°C. Additionally, because the size of the helical taper is greatly small, which is only a few hundred micrometers, the thermal expansion and thermo-optic effects have little influence on it. Therefore, asshown in Fig. 5, with the increasing of temperature, the transmission wavelength of Dip A hardly changes. The inset shows the relationship between temperature and the transmission wavelength, and there is a very small wavelength fluctuation of 0.72nm with the temperature varies from room temperature to 100°C, which can be neglected for torsion measurement. Therefore, we can consider that this torsion sensor is almost insensitive to temperature, and it solves the problem of torsion-temperature cross sensitivity greatly.

V. Conclusions

We propose and experimentally demonstrate a novel helical taper structure, which was fabricated in panda polarization-maintaining fiber for torsion and temperature sensing. The optimal taper parameters are the waist diameter of 60.84 μm and the length of 700 μm. And the helical taper was fabricated by an electric-arc discharge method. Experimental results demonstrate that the torsion sensitivity can reach up to −3.191 nm/(rad/m) when twisted the helical taper in clockwise, which is relatively higher than the previous proposed torsion sensors. Additionally, it is able to measure twist rate and identify rotational direction simultaneously. Furthermore, the torsion sensor is almost insensitive to temperature, and it solves the problem of torsion-temperature cross sensitivity greatly in the practical applications.

References

[1] Z. Tian, S. S.-H. Yam, and H.-P. Loock, "Refractive index sensor based on an abrupt taper Michelson interferometer in a single-mode fiber," *Opt. Lett.*, vol. 33, no. 10, pp. 1105–1107, 2008.

[2] K. Ren, L. Ren, J. Liang, X. Kong, H. Ju, and Z. Wu, "Highly strain and bending sensitive microtapered long-period fiber gratings," *IEEE Photon. Technol. Lett.*, vol. 29, no. 13, pp. 1085–1088, Jul. 1, 2017.

[3] S. Turtaev, I. T. Leite, T. A. Boussac, J. M. P. Pakan, N. L. Rochefort, and T. Cižmár, "High-fidelity multimode fibre-based endoscopy for deep brain *in vivo* imaging," *Light Sci. Appl.*, vol. 7, no. 1, 2018, Art. no. 92.

[4] B. Rahmani, D. Loterie, G. Konstantinou, and C. Moser, "Multimode optical fiber transmission with a deep learning network," *Light Sci. Appl.*, vol. 7, Oct. 2018, Art. no. 69.

[5] G. Wang *et al.*, "Ship hull structure monitoring using fibre optic sensors," *Smart Mater. Struct.*, vol. 10, no. 3, pp. 472–478, 2001.

[6] K. Ren, L. Ren, J. Liang, X. Kong, H. Ju, and Z. Wu, "Online and efficient fabrication of helical long-period fiber gratings," *IEEE Photon. Technol. Lett.*, vol. 29, no. 14, pp. 1175–1178, Jul. 15, 2017.

[7] F. Zhang *et al.*, "Highly sensitive torsion sensor based on directional coupling in twisted photonic crystal fiber," *Appl. Phys. Express*, vol. 11, no. 4, 2018, Art. no. 042501.

[8] R. Subramanian, C. Zhu, H. Zhao, and H. Li, "Torsion, strain, and temperature sensor based on helical long-period fiber gratings," *IEEE Photon. Technol. Lett.*, vol. 30, no. 4, pp. 327–330, Dec. 15, 2017.

[9] M. Bianchetti *et al.*, "Symmetric and asymmetric core-offset Mach–Zehnder interferometer torsion sensors," *IEEE Photon. Technol. Lett.*, vol. 29, no. 18, pp. 1521–1524, Sep. 15, 2017.

[10] Q. Fu *et al.*, "Intensity-modulated directional torsion sensor based on in-line optical fiber Mach–Zehnder interferometer," *Opt. Lett.*, vol. 43, no. 10, pp. 2414–2417, 2018.

[11] X. Li *et al.*, "Helical fiber interferometer using flame-heated treatment for torsion sensing application," *IEEE Photon. Technol. Lett.*, vol. 29, no. 1, pp. 161–164, Jan. 1, 2017.

[12] Y. P. Wang and Y. J. Rao, "Long period fibre grating torsion sensor measuring twist rate and determining twist direction simultaneously," *Electron. Lett.*, vol. 40, no. 3, pp. 164–166, 2004.

[13] X. Cao, D. Tian, Y. Liu, L. Zhang, and T. Wang, "Sensing characteristics of helical long-period gratings written in the double-clad fiber by CO_2 laser," *IEEE Sensors J.*, vol. 18, no. 18, pp. 7481–7485, Sep. 2018.

[14] Q. Zhou *et al.*, "Fiber torsion sensor based on a twist taper in polarization-maintaining fiber," *Opt. Exp.*, vol. 23, no. 18, pp. 23877–23886, Sep. 2015.

[15] F. Tan, Z. Liu, J. Tu, C. Yu, C. Lu, and H.-Y. Tam, "Torsion sensor based on inter-core mode coupling in seven-core fiber," *Opt. Express*, vol. 26, no. 16, pp. 19835–19844, 2018.

[16] Z. Bai *et al.*, "Torsion sensor with rotation direction discrimination based on a pre-twisted in-fiber Mach–Zehnder interferometer," *IEEE Photon. J.*, vol. 9, no. 3, Jun. 2017, Art. no. 7103708.

[17] W. Chen, S. Lou, L. Wang, H. Zou, W. Lu, and S. Jian, "Highly sensitive torsion sensor based on Sagnac interferometer using side-leakage photonic crystal fiber," *IEEE Photon. Technol. Lett.*, vol. 23, no. 21, pp. 1639–1641, Nov. 2011.

[18] Y. Jung, G. Brambilla, and D. J. Richardso, "Polarization-maintaining optical microfiber," *Opt. Lett.*, vol. 35, no. 12, pp. 2034–2036, 2010.

[19] X. Wang *et al.*, "Polarization-maintaining property of tapered polarization-maintaining fibers," *Appl. Opt.*, vol. 52, no. 8, pp. 1550–1554, 2013.

[20] D. Guilan, C. Caihe, Z. Delong, and C. Yuming, "Test investigation on fast and slow birefringence axes orientation for single-mode polarization-maintaining optical fiber," *J. Tianjin University.*, vol. 32, no. 5, pp. 633–636, 1999.

[21] H. Zhang *et al.*, "Directional torsion and temperature discrimination based on a multicore fiber with a helical structure," *Opt. Express*, vol. 26, no. 1, pp. 544–551, 2018.